Design of cellular steel beams subjected to lateral torsional buckling

Nicolas Boissonnade, Joanna Nseir, Hugues Somja

Design of cellular steel beams subjected to lateral torsional buckling

Nicolas Boissonnade, Joanna Nseir and Hugues Somja.

Nicolas Boissonnade, Professor, Civil Engineering Department, Laval University, Québec Canada, Nicolas.boissonnade@gci.ulaval.ca

Joanna Nseir, Professor, Civil Engineering Department, University of Applied Sciences of Western Switzerland, Fribourg, Switzerland, joanna.nseir@hefr.ch

Hugues Somja, Professor, Institut National des Sciences Appliquées, Rennes, France, Hugues.Somja@insa-rennes.fr

Highlights

- The results of more than 4 000 non-linear shell F.E. computations are presented, detailed and analysed;
- Prior to the numerical parametric studies, the numerical models were validated against test data on full-scale specimens, as detailed in the companion paper;
- Various parameters such as the base cross-section profile, the bending moment distribution, the size and position of the openings, the steel grade and member slenderness have been studied;
- Besides, a dedicated design model is presented. Systematic comparisons with the results of software ACB+, which is by far the most highly used tool in design practice, are described;
- A significantly improved performance of the proposed design approach in terms of accuracy, consistency and reliability is demonstrated.

Abstract

The present paper investigates the lateral torsional buckling resistance of cellular steel beams numerically. Such beams are quite sensitive to lateral instability owing to a substantial increase in depth of the cross-section with respect to the base profile. While a companion paper [1] was dedicated to (i) characterising experimentally the behaviour of cellular and Angelina beams and to (ii) validating dedicated non-linear shell F.E. models, this paper details the results of extensive numerical studies. Several key parameters in the structural response are investigated, such as the base cross-section profile, bending moment distribution, size and position of the openings, steel grade and member slenderness.

The results have further been used to assess an original design proposal for the lateral torsional buckling resistance of such girders. The improved design rules are shown to provide accurate yet safe ultimate load predictions. Also, in comparison with existing and available design rules, the proposal is seen to allow for substantially higher design loads – still safe-sided –, potentially leading to significant material savings.

1. Introduction

This paper is dedicated to the Lateral Torsional Buckling (L.T.B.) of cellular steel beams. Such beams are usually characterized by (i) a high height-to-width h / b ratio as well as by (ii) long spans, so that characterizing their response to L.T.B. is of prime importance for an appropriate design. In particular, it was shown in a companion paper [1] that corresponding failure modes may span from inelastic to elastic L.T.B., such as in usual steel beams. Accordingly, many "classical" parameters have an influence: unbraced length, bending moment distribution, conditions of lateral bracing, etc.; in addition, the effects of the regularly-spaced circular openings is to be characterized.

As proven very effective to resist bending actions, cellular girders have received specific attention in the recent decades. Several authors focused on the determination of the critical moment in cellular and castellated beams [2]-[4], on distortion [5] or on mode interactions [6], flexural buckling [7]-[9], beam-column behaviour [10]-[12], web post local buckling [13], [14], resistance under fire [15], on the influence of residual stresses [16]-[18], etc. Closer to the topic of the present paper, investigations by Panedpojaman et al. [19] report important shear-moment interactions affecting the section resistance of cellular beams, in addition to studying the influence of Virendeel effects. Recent years have also seen efforts towards the use of artificial neural network or related numerical techniques [20]-[23] to provide flexural buckling or L.T.B. resistance estimates.

Nevertheless, to this date, no L.T.B. design procedure has been widely recognized nor accepted as the most effective, accurate and safe approach. Although the above-referenced research papers have brought significant insights on the behaviour and response of cellular beams, major design standards still provide very different design provisions, if any (e.g., [24]). In this respect, the

present paper investigates numerically the L.T.B. behaviour and structural response of such beams and suggests new design recommendations. First, the paper details how validated shell F.E. models ([1]) have been extended and adapted to lateral torsional buckling reference situations, namely with respect to "ideal" fork support conditions. Modelling details such as initial geometrical imperfections are also discussed (see Section 2). Then, Section 3 details all the considered parameters in an extensive parametric study leading to some 4 000 non-linear F.E. results. Key factors such as the base cross-section profile, the bending moment distribution, the size and position of the openings, the steel grade and member slenderness have been considered. These reference results have served assessing the merits of a new design proposal presented in Section 4, where the proposal is in particular compared to current state-of-the-art design recommendations.

2. F.E. modelling

2.1 Material – Support condition and loading

The developed F.E. models being shown to be adequate [1], adapted numerical models have been derived, on the basis of the validated ones and are described hereafter. Similar modelling features were adopted, and all mapped meshes used herein were shown beforehand to be adequate, namely regarding mesh density, aspect ratios and distortion. As a particular point, advanced characteristics for the web-flange areas have been adopted here as well, namely the use of (i) extra beam elements so as to match nearly exactly the cross-section geometrical properties and of (ii) truss elements to ensure that the web-flange areas remain free from local buckling.

Modifications to the boundary conditions so as to fulfil so-called "fork support conditions" have also been implemented; accordingly, the torsional twist was prevented and warping left free at the

end-sections. In this respect, the following two main modifications were brought to the end sections:

(i) As vertical stiffeners were no more considered, additional support conditions were used in order to prevent local buckling; this was made effective in fixing the corresponding out-of-plane displacements of the concerned nodes in both flanges and web (cf. Fig. 1a);

(ii) Simultaneously, linear kinematic constraints were adopted to ensure that the end sections, modelled by means of shell elements, behave as in a beam-like F.E. modelling. This was primarily intended at keeping the obtained shell models' results "compatible" with code recommendations, which for the most part bear a beam theory background. With respect to the longitudinal displacements of the end-sections nodes (*x*-axis, see Fig. 1a), constraints relationships have been defined between these nodes so that the end sections to exhibit a maximum of 4 global cross-sectional displacement modes (see Fig. 1b), namely (i) (global) axial displacement, (ii) rotation about major-axis with plane-sections-remain-plane assumption, (iii) equivalent minor-axis rotation and (iv) warping displacements in the flanges – more details relative to this particular numerical modelling can be found in [25].

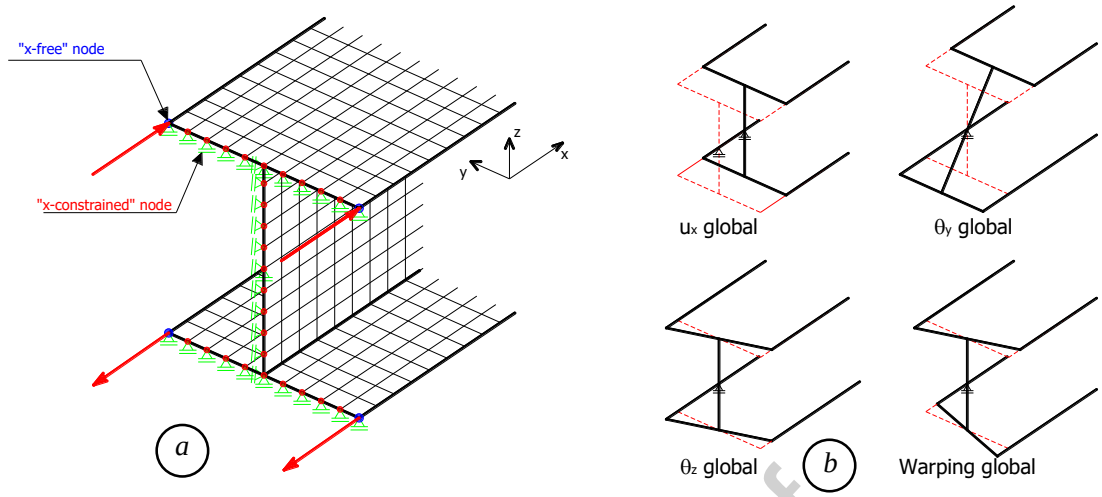

Fig. 1. a) Support conditions and application of loading – b) End section global deformation modes.

For sake of symmetry, the four nodes at the flanges' tips have been chosen as the "*x*-free" ones, and all other nodes are consequently the "*x*-constrained" ones. Doing so allows for a satisfactory treatment of the global behaviour of the end sections, given the levels of displacements and rotations reached within the present study. It also avoids the use of additional rigid elements superposed along the flanges and webs of the end-sections ([26]), which aim at preventing local instabilities and tempering stress concentrations but may cause numerical issues. This modelling technique has been shown to be very effective ([25], [27], [28]), and was validated and adopted in many F.E. studies.

The application of any external loading at the member's ends (i.e., major and minor-axis bending moments and/or axial forces) is straightforward and has been implemented by means of suitable sets of nodal forces at the flanges' tips (see Fig. 1a). As a further feature of the adopted kinematic relationships, this way of introducing end moments and forces can be shown to avoid any unintended stress concentrations. It should also be recalled here that special attention was paid to the numerical modelling of the web-flange junction in order to ensure the required cross-sectional properties with respect to the original cross-section [1].

Typical elastic-perfectly plastic with strain hardening constitutive laws have been adopted (Fig. 2), and use of nominal values of the yield stress has been made in the parametric numerical studies. The maximum admissible strain ε_{max} adopted in all simulations was set at 10%. Table 1 gives further data relative to the constitutive model used in the numerical simulations.

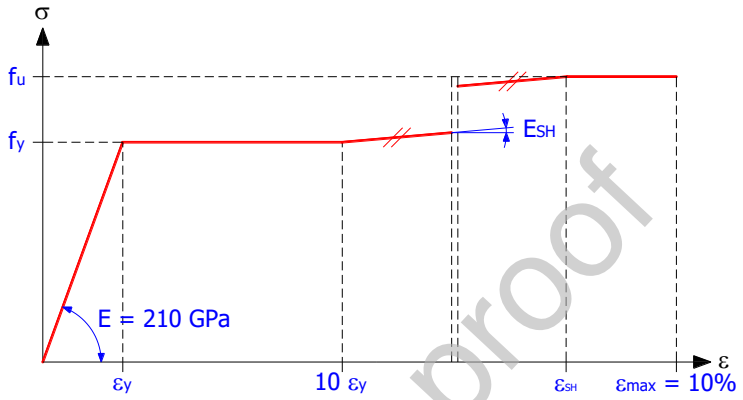

Fig. 2. Stress-strain relationship used in F.E. parametric studies.

Table 1. Characteristics of the material models used in numerical studies.

	f_y $[N/mm^2]$	f_u $[N/mm^2]$	ε_y [%]	ε_{SH} [%]	ε_{max} [%]	E_{SH} $[N/mm^2]$
S235	235	360	0.112	4.096	10	4200
S460	460	550	0.219	4.333	10	4200

As a specific point of geometrical modelling, decision was made to use plain panels at the beams' extremities having a fixed length equal to 0.5 *s*, as shown in Fig. 3. The intention was to avoid the possible local failure modes at the end of the members, which lay out of the scope of the present study.

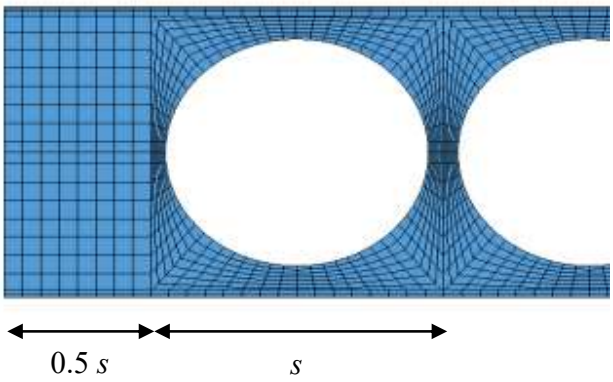

Fig. 3. Plain web panel of length 0.5 *s* as end segment of cellular beam.

2.2 Initial imperfections

Initial *geometrical* imperfections have been accounted for by means of adequate modifications of node coordinates. A combination of both global and local imperfections has been introduced, as follows:

- *Global* imperfections have been considered as the combination of a lateral sinusoidal imperfection with amplitude L / 500 and of an initial torsional twist with maximum amplitude at mid-span equal to L / (2000 H) where L is the total length of the member – see also Figs. 4a and 4b, as well as [29]. These amplitude values are known to be a little high compared to measurements but have been adopted to include the influence of residual stresses in an indirect way;
- *Local* imperfections allowing the potential development of local instabilities on the member's behaviour have been defined as square half-wave patterns in both directions of the flanges and of the webs, with an amplitude of a / 400, where a designates the flat width of the flange or of the web – the latter amplitude is based on recommendations from [24] and [30]. Specifically for webs, sinusoidal "S-shape" distributions have been adopted (see Fig. 4c): this pattern is inherent to the fabrication process (welding at mid-height of

the web) and is typically observed for cellular beams – it also remains the most unfavourable imperfection shape of the web with respect to a potential shear buckling failure at the end sections.

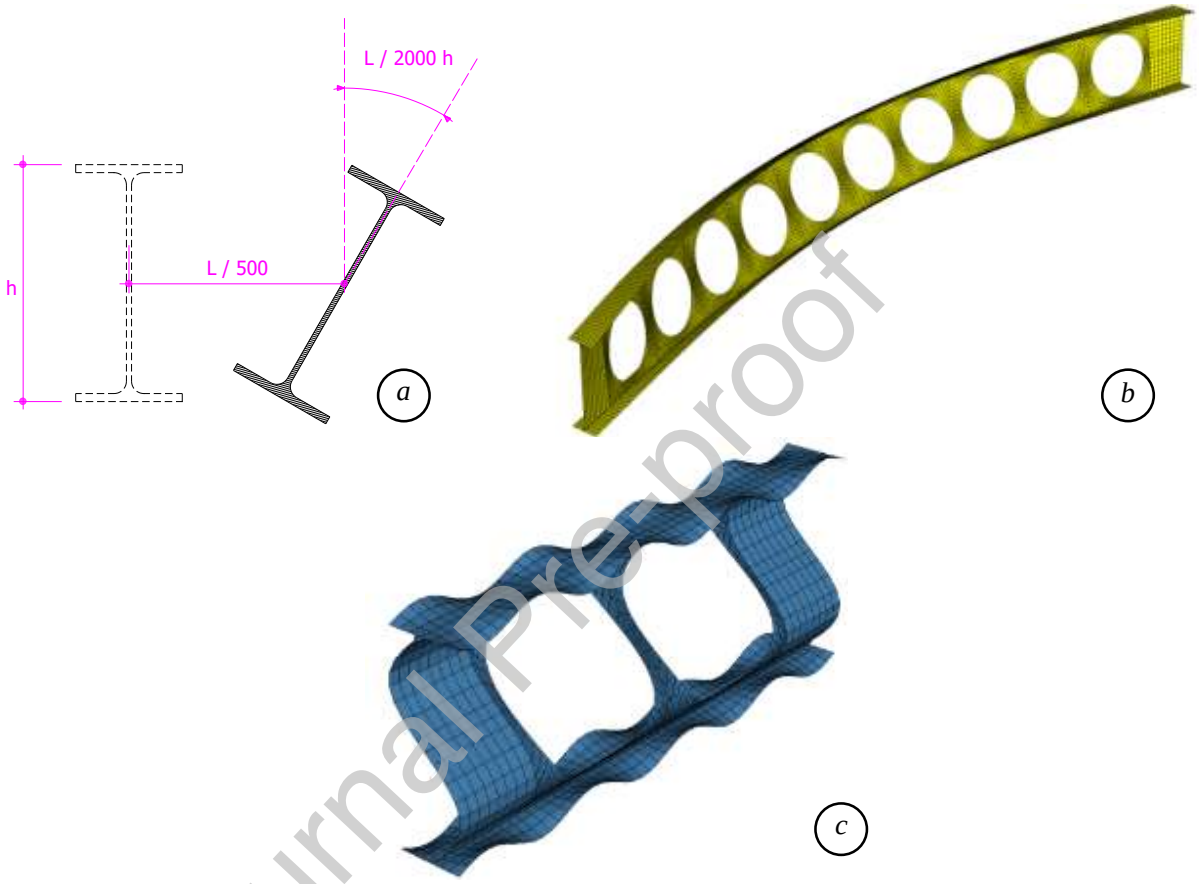

Fig. 4. Standard geometrical imperfections patterns – a) Amplitudes for global imperfections – b) Member global imperfection (magnified) – c) Local "plate" and "S-shape" imperfections in flanges and web (magnified).

It is to be noted that the definition of the local imperfections in the web was kept fully independent from that of the flanges. Also, it shall be mentioned that local imperfections have been defined so as to leave the web-to flange region free from local imperfections; this area is indeed assumed to remain rigid during loading, even in cases where local buckling develops (see details on the modelling of the web-flange area in [1]).

No residual stresses have been included in the numerical simulations since their actual distribution is relatively difficult to predict in a systematic way, owing to the industrial manufacturing process ([16], [17]). Their detrimental influence is assumed as being indirectly accounted for through higher amplitudes in the geometrical imperfections and their combination, as explained before.

3. Numerical parametric studies

3.1 Parameters considered

The developed F.E. models have been extensively used within parametric studies collecting reference results for the assessment of an appropriate design proposal. The various parameters accounted for in these parametric studies have been chosen so as to represent closely the whole set of potential practical applications. Further, production, erection and service constraints have been taken into account in the selection of the parameters' values. Accordingly, the following set of parameters has been considered in the numerical studies with typical fork conditions and elastic-perfectly plastic constitutive laws:

- 6 base profiles geometries ("parent sections") have been considered, from small to large, either closer to column shapes (HEs) or to beam shapes (IPEs): IPE 300, IPE 400, IPE 600, HEA 400, HEB 800 and HEM 1000;
- 4 values of parameter s, characterizing the relative size of the openings: $s = 1.12\ a_0$, $s = 1.25\ a_0$, $s = 1.50\ a_0$, $s = 1.75\ a_0$ (see Fig. 6). Small values of s are usually relative to large openings with respect to the height of the final girder and find applications for light, roof beams with little material in the web posts between consecutive holes, while larger values of s indicate stockier beams, frequently used as floor beams;
- 2 steel grades: S235 and S460;

- 8 different values of the member length L leading to regular L.T.B. relative slenderness values λ_{LT} in typical $\chi_{LT} - \lambda_{LT}$ plots. L values were chosen so as to collect results for rather short beams ($\lambda_{LT} \approx 0.3$) and for quite long ones ($\lambda_{LT} > 2.0$). All beam lengths have however been chosen so as to remain realistic for practical applications;
- 5 bending moment distributions through 5 different load cases (LCs, Fig. 5): constant bending moment ($\psi = 1.0$, where ψ designates the end-moments ratio ($-1 \leq \psi \leq 1$) – load case 1 LC1), linear distributions ($\psi = 0$ – LC2 and $\psi = 0.5$ – LC5), concentrated load at mid-span (applied on top flange – LC3) and uniformly distributed transverse load (applied on top flange – LC4).

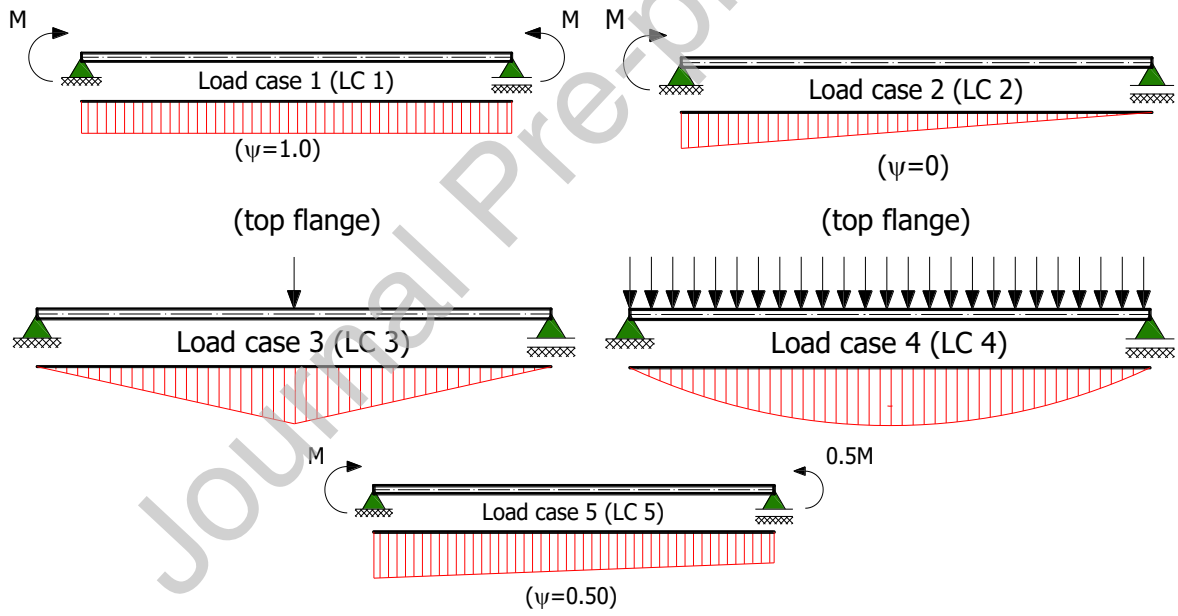

Fig. 5. Load cases considered in the parametric study.

L.B.A. (Linear Buckling Analysis) and G.M.N.I.A. (Geometrically and Materially Non-linear Analysis with Imperfections) numerical simulations have been performed for all cases. L.B.A. calculations aim at obtaining accurate estimates of the critical bending moment M_{cr} while G.M.N.I.A. analyses provide ultimate capacities, i.e., account for yield extent, local and global

buckling effects, imperfections and all interactions. The results of nearly 4 000 F.E. shell non-linear simulations are analysed in the following; these reference results have been further used for the assessment of the proposed design rules, as detailed in Section 4.

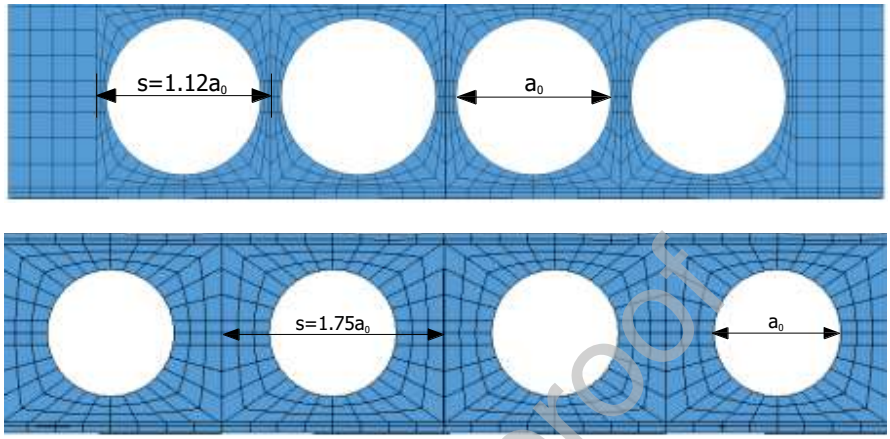

Fig. 6. Definition of s and a_0 parameters.

Fig. 7 provides an overall view of all collected numerical results, in classical $\chi_{LT} - \lambda_{LT}$ axes, where λ_{LT} is the relative L.T.B. slenderness (see Eq. (2) for definition) and χ_{LT} is a so-called "buckling reduction factor" (Eq. (3)) that is such that $\chi_{LT} \leq 1.0$ values indicate a detrimental influence of L.T.B. on the maximum carrying capacity. As an example, a $\chi_{LT} = 0.70$ value indicates that only 70% on the section's resistance in bending shall be accounted for, owing to L.T.B. causing a 30% reduction in resistance, i.e., the beam may only reach 70% of the section's carrying capacity. χ_{LT} therefore represents a direct measure of the girder's resistance as affected by L.T.B. Fig. 7 also shows that although the resistance to L.T.B. appears to remain only slightly affected by the steel grade, the relatively large scatter observed indicates that many parameters have an important influence on the girders' responses and shall be studied in detail. In this respect, various trends are identified and presented in Figs. 8 to 10, in order to isolate key and leading parameters on the L.T.B. resistance that shall be paid due account in any design approach.

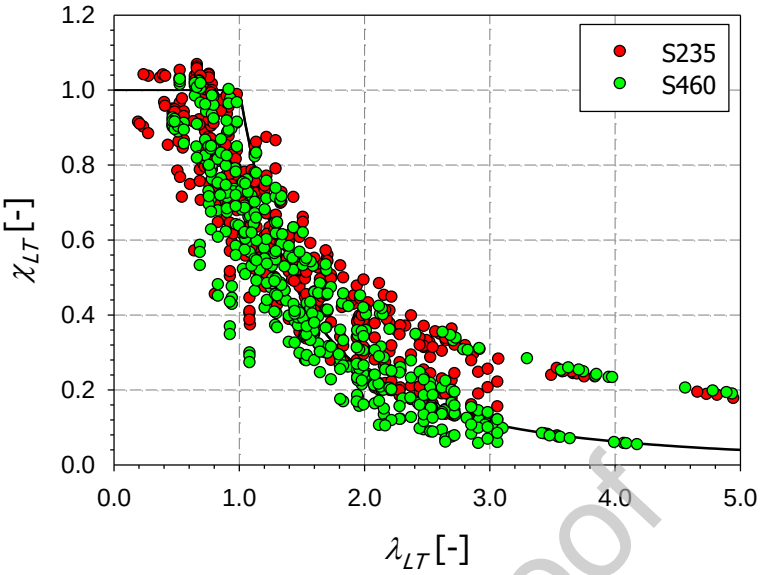

Fig. 7. Overall plot of all numerical results.

3.2 Analysis of results and trends

All results in Figs. 8 to 10 are presented in $\chi_{LT} - \lambda_{LT}$ axes; they also report $\chi_{LT} = 1.0$ lines that represent a "resistance limit" of the girders (i.e., full section capacity is reached in the absence of L.T.B.), as well as "stability limit" curves – Euler hyperbola – that are relative to a perfect member buckling behaviour (i.e., no yield limit nor imperfections). These two ideal responses represent upper bounds of the real members' resistance to L.T.B. $\chi_{LT} \geq 1.0$ results may however be observed, mostly as a consequence of strain hardening effects; the latter influence is however limited. Also, it may be noticed in these figures that some results for high λ_{LT} values (long beams) are reported to lie above the so-called "Euler curve": this may be explained by the fact that (i) for such long members, the observed levels of curvature are such that some assumptions on which the classical linear buckling "Euler" theory relies may no longer be fulfilled (e.g., small rotations) and (ii) because the corresponding profiles may partially mobilize minor-axis resistance, some cross-sections being significantly twisted about their longitudinal axis. This latter influence is well-known and usually observed for HE-type sections since their relative

minor-axis resistance are greater than that of deeper IPE-type sections. In this respect, Figs. 8a and 8b also draw $\chi_{LT} = W_{pl,z} / W_{pl,y}$ horizontal limits which represent the χ_{LT} value reached when minor-axis plastic resistance is attained, for the sections concerned.

3.2.1 Influence of bending moment distribution

Figs. 8a and 8b first present a series of results on IPE 600 and HEB 800 parent sections, under various load cases and for two different steel grades. Intention is here to investigate in which extent the parent section general dimensions influence the resistance to major-axis bending. For a given parent section, Figs. 8a and 8b show that relatively similar trends are observed, except at low and intermediate λ_{LT} slenderness where more sensitivity to the load case is visible – imperfections and interactions with yielding indeed have more influence here. Similar observations for standard hot-rolled wide flange profiles are usually observed, and appropriate design rules have been proposed (e.g., [24]), as a function of the bending moment distribution. Also, Fig. 8a and 8b show little influence of the yield limit on the response to L.T.B. since very similar trends and values are observed when comparing these two figures.

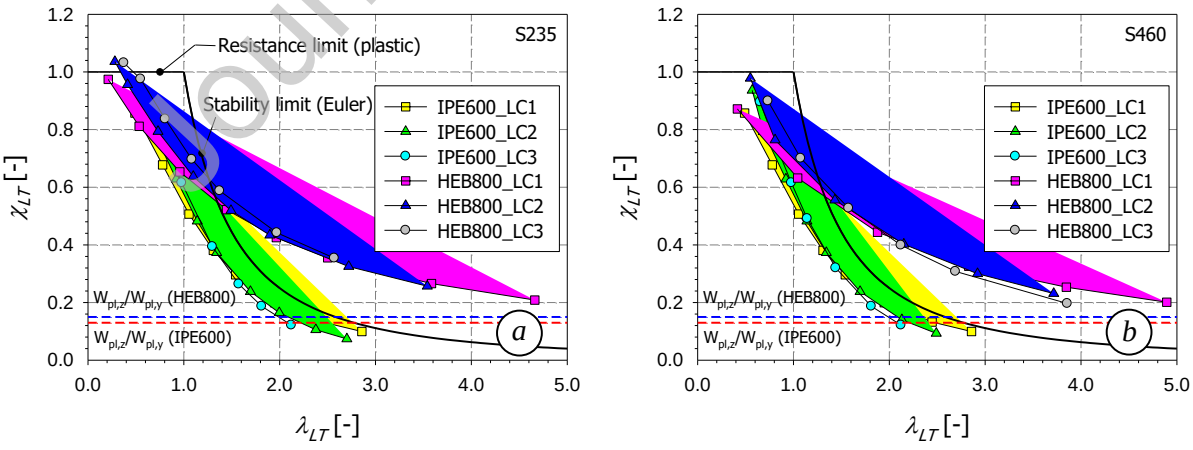

Fig. 8. Influence of bending moment distribution (girders with IPE 600 and HEB 800 base profiles, $s = 1.50\ a_0$) – a) S235 – b) S460.

3.2.2 Influence of cross-section geometry

Yet, Fig. 8a and 8b display a rather different behaviour for IPE base profiles compared to HEB base profiles, whatever the load case or steel grade considered. Although some standards (e.g., Eurocode 3 [24]) may distinguish L.T.B. responses of sections having height-to-width h / b ratios lower than 2.0 (usually HEs) from h / $b \geq 2.0$ ones (IPEs), values reported in Table 2 indicate that this parameter is not responsible for the differences observed here for cellular beams: h / b ratios are quite close for both parent and final sections. Also, the relative importance of minor vs. major-axis resistance and stiffness remain similar, as indicated by $W_{pl,z}$ / $W_{pl,y}$ and I_y / I_z ratios.

Table 2. Geometrical and mechanical characteristics of profiles with IPE 600 and HEB 800 parent sections.

Parent section	h_{parent} / b [–]	h_{ACB} / b [–]	t_f / t_w [–]	$W_{pl,z}$ / $W_{pl,y}$ [–]	I_y / I_z [–]	I_y / I_t [–]
IPE 600	2.73	3.91	1.58	0.13	27.2	558
HEB 800	2.67	3.83	1.89	0.15	24.1	373

One may however notice relative stronger flanges in the case of the HEB 800 parent section, and this has consequences mainly on torsional characteristics (Saint Venant's torsional inertia I_t), as shown by quite different I_y / I_t ratios. For long members, the Saint Venant's torsional stiffness $G\,I_t$ bears most of the resistance to torsion, which leads to HE sections resisting better to torsional twist and thus recording less torsional twist at peak. Consequently, long HEB 800 parent sections girders experience relatively higher in-plane, major axis curvature than their IPE 600 counterparts, so that the former are more prone to lying above the Euler curve, as previously detailed. Such a different behaviour is again visible in many of the following results.

3.2.3 Influence of relative size of openings

Figs. 9a and 9b investigate the influence of parameter *s* that characterizes the amount of material present between consecutive holes (see Fig. 6 for examples of extreme practical values $s = 1.12\ a_0$ and $s = 1.75\ a_0$). As can be seen, for a given parent section and load case, changes in *s* do not alter the observed L.T.B. resistance trends, although affecting the values of λ_{LT} and the associated χ_{LT} reduction factors. Therefore, as soon as the presence of holes is accounted for through adequate λ_{LT} and χ_{LT} pairs, parameter *s* can conveniently be omitted from the definition of the L.T.B. resistance curve. Also, as a comparison between Fig. 9a and 9b shows, the influence of *s* on the response to different load arrangements remains negligible, provided correctly accounted for in the L.T.B. curve – yet observe that design curves shall be different for $\psi = 1$ than for $\psi = 0$ cases. Fig. 10a and 10b further evidence identical trends and conclusions for an IPE 800 base section, confirming the independence of the resistance curve to parameter *s* for other section shapes.

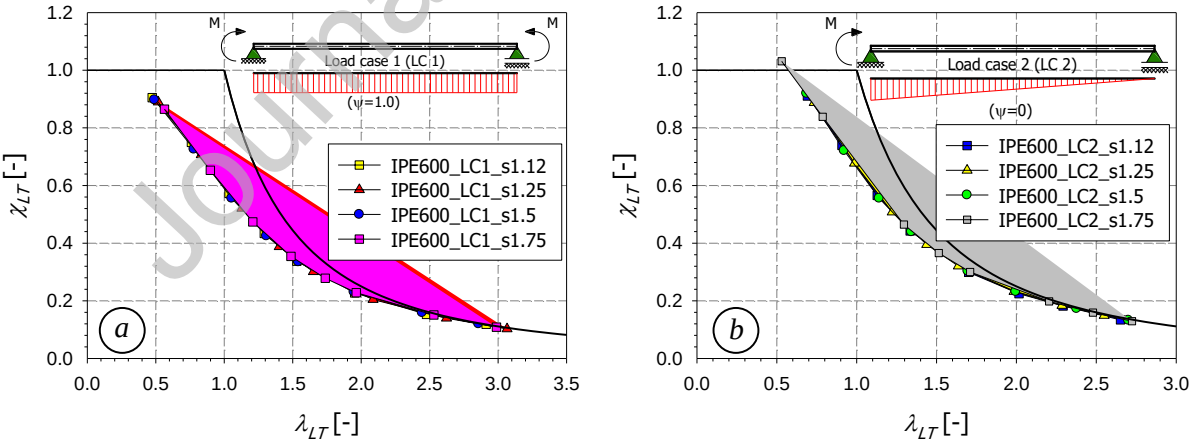

Fig. 9. Influence of the relative size of web openings (factor *s*), IPE 600, S235 – a) Constant bending moment – b) Triangular bending moment.

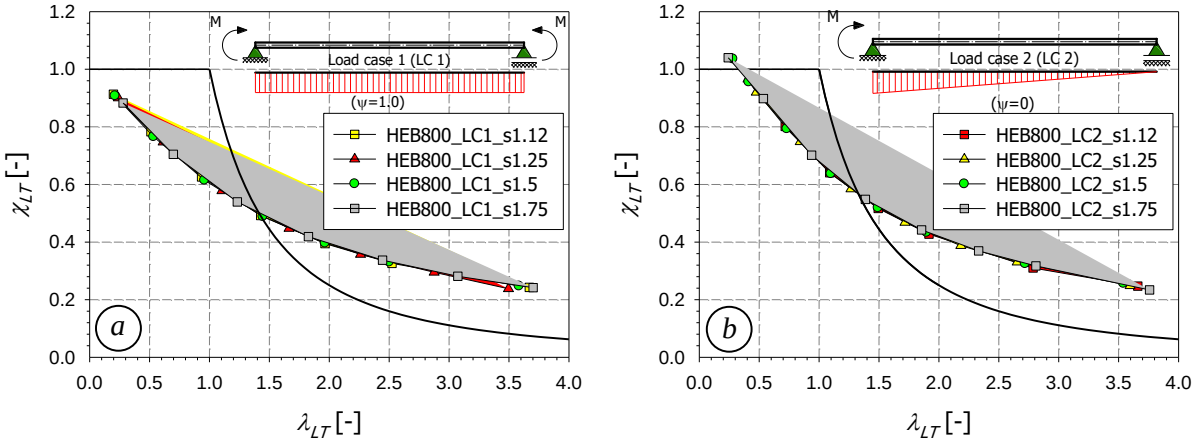

Fig. 10. Influence of the relative size of web openings (parameter s), HEB 800, S235 – a) Constant bending moment – b) Triangular bending moment.

4. Proposal for new design rules

4.1 Improved design rules

As briefly recalled in the introduction (see also [1] for a deeper literature review), state-of-the-art design rules against L.T.B. failure found in main design standards usually assume the resistance of the cellular girder to be that of the Tee in compression. In particular, highly-used design software ACB+, hereafter referred to as "ACB+" ([31]), is based on such an approach; since ACB+ is by far the most highly used tool in design practice, it will be kept as a reference in the following. ACB+ design procedure basically consists in assuming that the girder's resistance to lateral buckling can be calculated as the lateral buckling resistance of the "Tee" in compression of the weakest cross-section (section A-A in Fig. 11). This Tee is considered as acted by compressive forces only, and is therefore verified against lateral buckling, with a buckling length set equal to the length between points of lateral support. The corresponding design check then reads as in Eq. (1).

$$\frac{N_{Ed}}{N_{b,Rd}} \le 1.0 \quad \text{or} \quad \frac{M_{y,Ed}}{M_{b,Rd}} \le 1.0 \quad \text{with} \quad M_{b,Rd} = N_{b,Rd} \cdot d_{Tees} \tag{1}$$

In Eq. (1), N_{Ed} refers to the axial compression force in the upper "Tee", $N_{b,Rd}$ to the lateral buckling resistance of the Tee and d_{Tees} to the distance between respective centroids of the Tees. Even if the actual bending moment distribution on the member may possibly be considered by means of a variable level of axial compression in the Tee along the unrestrained length, this design proposal can be shown to lead to very conservative estimates of the lateral torsional buckling resistance, mainly because:

- The stabilising effect of the tension flange is fully neglected;
- The torsional stiffness of the cross-section is also disregarded;
- Considering the Tee of the weakest cross-section neglects the material in-between consecutive holes; this, in many cases, may have an important influence, as will be shown in the following (e.g., in the case of typical "floor" beams where *s* is large).

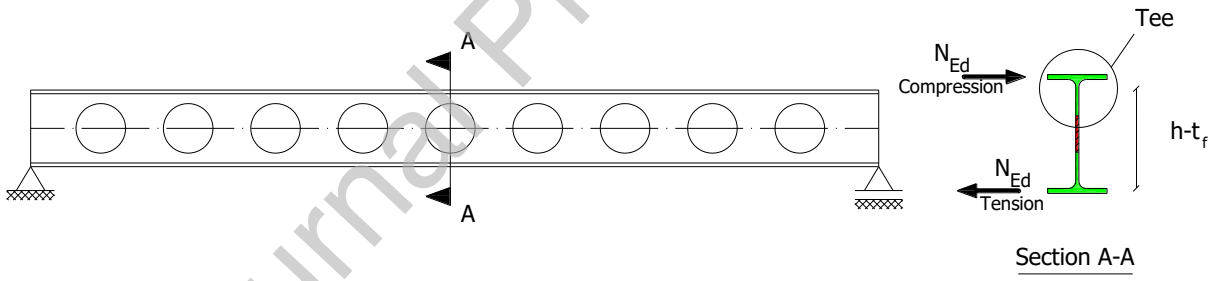

Fig. 11. Tension and compressions Tees in a cross-section at the middle of a hole.

In order to improve this situation, several design models have been built and tested, and the best compromise between consistency, simplicity and accuracy has been achieved through a very similar approach to that of the actual rules of Eurocode 3 ([24]) for the lateral torsional buckling of standard profiles. The procedure however makes use of the weakest cross-section properties and adopts buckling curve "*c*" for IPE sections and curve "*d*" for HE sections. The proposed design approach then consists in the following steps:

1. Determine the section properties of the *weakest cross-section* (i.e., at the centre of an opening): $M_{y,Rk}$, I_z, I_t, I_ω – all usual section properties, and $M_{y,Rk}$ represents the characteristic cross-section resistance to major-axis bending;
2. Calculate the elastic critical bending moment M_{cr}, on the basis of these properties through classical expressions found in textbooks or in Eurocode 3 [24] for example;
3. Evaluate the relative slenderness to lateral torsional buckling λ_{LT}:

$$\overline{\lambda}_{LT} = \sqrt{\frac{M_{y,Rk}}{M_{cr}}} \tag{2}$$

4. Determine the reduction factor due to lateral torsional buckling λ_{LT} with the use of Eurocode 3 buckling curve "*c*" for IPE sections and curve "*d*" for HE sections, (see ([24]):

$$\chi_{LT} = \frac{1}{\phi_{LT} + \sqrt{{\phi_{LT}}^2 - {\overline{\lambda}_{LT}}^2}} \leq 1 \text{ where } \phi_{LT} = 0.5\left[1 + \alpha_{LT}\left(\overline{\lambda}_{LT} - 0.2\right) + {\overline{\lambda}_{LT}}^2\right] \tag{3}$$

5. Last, evaluate the lateral torsional buckling resistance $M_{b,Rd}$ as:

$$M_{b,Rd} = \chi_{LT}\frac{M_{y,Rk}}{\gamma_{M1}} \tag{4}$$

where γ_{M1} refers to the usual partial safety factor to be applied to the resistance of members subjected to instabilities. As suggested by Eurocode 3 [24] for regular I-beams, substitution of χ_{LT} by $\chi_{LT,\text{mod}}$ factor to better account for potential beneficial effects for non-constant bending moment distributions was also considered. Analytical predictions as based on $\chi_{LT,\text{mod}}$ have been considered in the following comparisons with numerical reference results.

It may easily be realized that relying on the weakest cross-section has a limited influence on the resistance to bending since the part of the ignored web barely changes the mechanical properties and response of the girder. However, the consideration of the cross-section as a whole (i.e., including the flange in tension) combined with a more correct warping stiffness can be shown to have a significant, positive impact on the obtained results. Also, the previously-identified trends (e.g., dependencies on load case, section shape and dimensions) can be seen to be all addressed within the proposed approach.

4.2 Validation of proposal against F.E. reference results

4.2.1 Influence of critical bending moment M_{cr}

Accuracy and consistency of the present design proposal has first been tested with respect to L.B.A. results, i.e., comparing reference, F.E.-obtained critical bending moment $M_{cr,FE}$ values to their predicted $M_{cr,proposal}$ counterparts. Tables 3 and 4 propose example sets of the obtained results, which, in general, have demonstrated an excellent level of agreement between the numerical and analytical results.

Table 3. Accuracy of proposal for L.B.A. calculations (base profile: IPE 600).

	Tot. nb of F.E. results	$M_{cr,FE}$ / $M_{cr,proposal}$ [–]			
		Min.	Max.	Mean	St. dev.
Load case 1	32	0.99	1.06	1.03	0.02
Load case 2	31	0.99	1.07	1.04	0.02
Load case 3	24	0.94	1.09	1.05	0.04
Load case 4	23	0.90	1.08	1.02	0.05
Load case 5	26	0.90	1.08	1.04	0.04
$s = 1.12\ a_0$	30	0.92	1.07	1.02	0.03
$s = 1.25\ a_0$	33	0.90	1.08	1.04	0.03
$s = 1.5\ a_0$	34	0.92	1.08	1.03	0.04
$s = 1.75\ a_0$	35	0.94	1.09	1.05	0.03

Table 4. Accuracy of proposal for L.B.A. calculations (all base profiles).

		Tot. nb of F.E. results	$M_{cr,FE}$ / $M_{cr,proposal}$ [–] Min.	Max.	Mean	St. dev.
HEB 800	Load case 1	32	0.93	1.03	1.00	0.02
	Load case 2	27	0.96	1.04	1.01	0.02
	Load case 3	23	0.97	1.06	1.03	0.02
	Load case 4	22	0.91	1.04	0.99	0.03
	Load case 5	25	0.94	1.05	1.02	0.03
HEA 400	Load case 1	30	0.92	1.02	1.00	0.02
	Load case 2	30	0.92	1.03	1.00	0.02
	Load case 3	27	0.97	1.05	1.03	0.01
	Load case 4	23	0.94	1.03	1.00	0.02
	Load case 5	27	0.91	1.04	1.02	0.02
HEM 1000	Load case 1	32	0.95	1.04	1.00	0.02
	Load case 2	29	0.93	1.04	1.01	0.02
	Load case 3	26	0.93	1.06	1.03	0.03
	Load case 4	24	0.92	1.05	1.01	0.03
	Load case 5	27	0.95	1.06	1.03	0.02
IPE 300	Load case 1	28	0.93	1.05	1.01	0.02
	Load case 2	29	0.93	1.06	1.02	0.03
	Load case 3	27	0.91	1.07	1.04	0.04
	Load case 4	22	0.92	1.07	1.01	0.04
	Load case 5	27	0.94	1.07	1.03	0.03
IPE 400	Load case 1	32	0.91	1.05	1.01	0.03
	Load case 2	31	0.94	1.05	1.02	0.02
	Load case 3	27	0.92	1.07	1.03	0.04
	Load case 4	24	0.93	1.06	1.01	0.04
	Load case 5	28	0.91	1.07	1.03	0.04
IPE 600	Load case 1	32	0.99	1.06	1.03	0.02
	Load case 2	31	0.99	1.07	1.04	0.02
	Load case 3	24	0.94	1.09	1.05	0.04
	Load case 4	23	0.90	1.08	1.02	0.05
	Load case 5	26	0.90	1.08	1.04	0.04

Considering the whole set of results, an average difference of 2% to 3% between both sources has been found, as well as very low standard deviations. This clearly indicates that the choice of the weakest cross-section is appropriate. Also, as the tables show, no load case sensitivity nor influence of the relative size of the openings could be evidenced. Too, no obvious influence of the base profile cross-section geometry can be shown, as Table 4 results show: $M_{cr,proposal}$ values

remain very close to the reference $M_{cr,FE}$ ones whatever the base cross-section, and very low standard deviations values reflect reliable, consistent estimates.

4.2.2 Resistance under constant bending moment ("reference case")

Referring now to ultimate load calculations (G.M.N.I.A. results), the proposed analytical model can also be shown to provide accurate predictions; Figs. 12 to 17 plot representative examples of results evidencing the improved accuracy, in comparison with reference "ACB+" results. The data are classically presented in terms of $\lambda_{LT} - \chi_{LT}$ plots (left), but also in terms of relative $\chi_{LT,FE}$ / $\chi_{LT,analytical}$ ratios with respect to the number of openings in the girder (right), which is another parameter closely linked to the length of the girder.

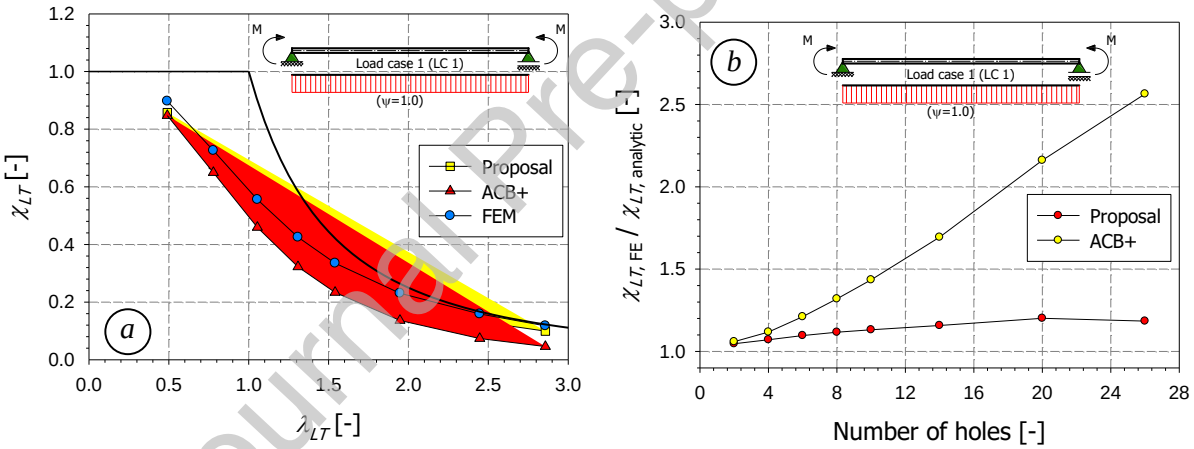

Fig. 12. Results for base profile IPE 600, constant bending moment, s = 1.5 a_0, S460, curve c.

In the particular case of an IPE 600 base section, Fig. 12a proposes a first comparison between ACB+ design recommendations and the proposed L.T.B. resistance model. Overall, the proposed design model is clearly seen to provide much closer solutions to the F.E. reference ones, especially for high λ_{LT} values. Indeed, for long beams, even if at first sight the ACB+ prediction may seem acceptable, it turns out to be quite severely underestimating the actual carrying capacity: for beams having 14 and more openings, which in the particular case considered here

leads to approximately 12 *m* elements[1], resistance predictions according to the proposed model remain about 15% on the safe side in average, while ACB+ results are seen to become very conservative, underestimating the real failure load by more than a factor 2. This latter observation is of particular relevance in practical situations involving composite cellular beams, since such high λ_{LT} values are usually met during the erection phase, owing to few – if any – intermediate points of lateral bracing. Given the associated low χ_{LT} values, the resistance to L.T.B. is of prime importance, and often leads the design – thus the need for improved design rules.

Figs. 13 to 17 report similar observations for other steel grades, relative sizes of the openings, load cases or parent sections, both qualitatively and quantitatively – in all cases, the ACB+ model for beams with more than 16 openings is systematically seen to provide results underestimating the reference F.E. resistance more than a factor 2.0, unlike the proposed approach that offers much better resistance predictions.

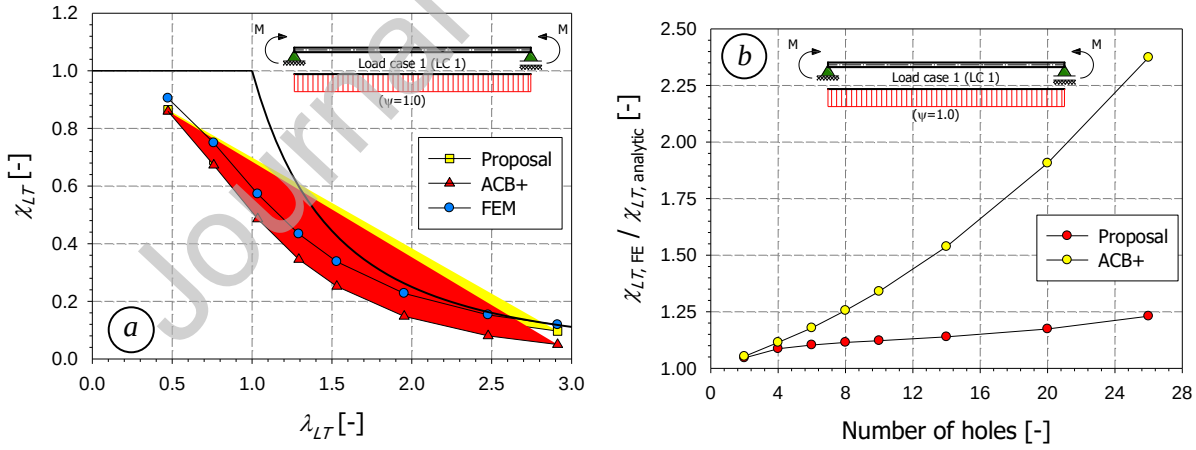

Fig. 13. Results for base profile IPE 600, constant bending moment, s = 1.12 a_0, S235, curve *c*.

[1] It is quite common to meet practical cellular beams spanning above 12 *m*, and up to 20 *m*.

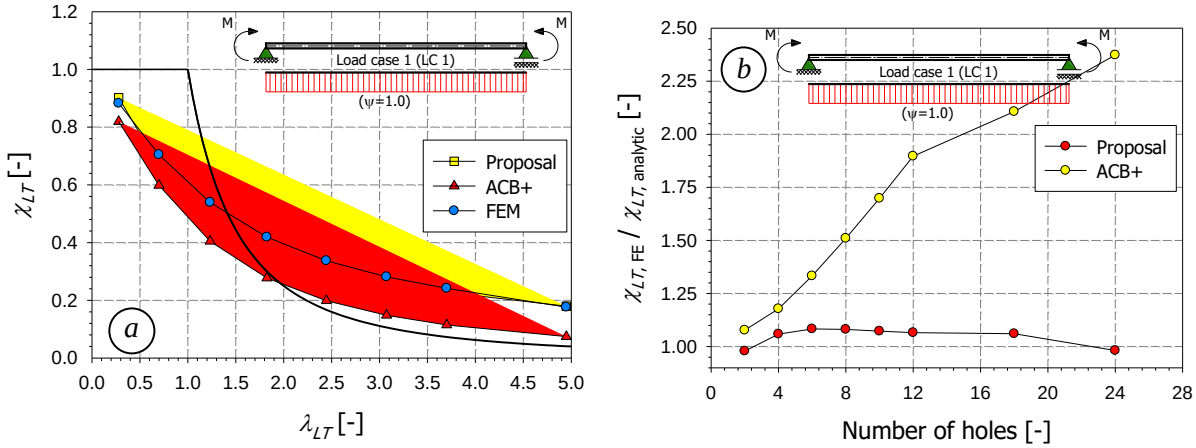

Fig. 14. Results for base profile HEB 800, constant bending moment, s = 1.75 a_0, S235, curve *d*.

Fig. 13, again relative to girders involving an IPE 600 parent section, proposes very close results and observations to Fig. 12 ones, however for a different steel grade and for comparatively larger openings (s = 1.12 a_0, meaning that thin posts between holes were considered – see also Fig. 6). Consequently, it can be concluded that the suggested model correctly accounts for these parameters through the suggested modifications of the λ_{LT} factor and provides satisfactory resistance estimates. Careful and details analysis of all collected F.E. results can also be shown to provide identical results and therefore yield similar conclusions – as another example, Fig. 14 shows results obtained for an HEB 800 parent section, with s = 1.75 a_0, i.e., much stronger webs between holes. The change in cross-section parent section in Fig. 14a and Fig. 14b is indeed seen to leave the good resistance predictions of the proposed design procedure unaffected.

4.2.3 Design under variable bending moment

Fig. 15a and Fig. 15b propose a first series of results with a different load case (LC2, triangular bending moment), which allows to investigate the ability of the proposed approach to account for another key parameter of L.T.B. Here again, results are seen to be very satisfactory, providing significantly more accurate resistance predictions than the ACB+ approach.

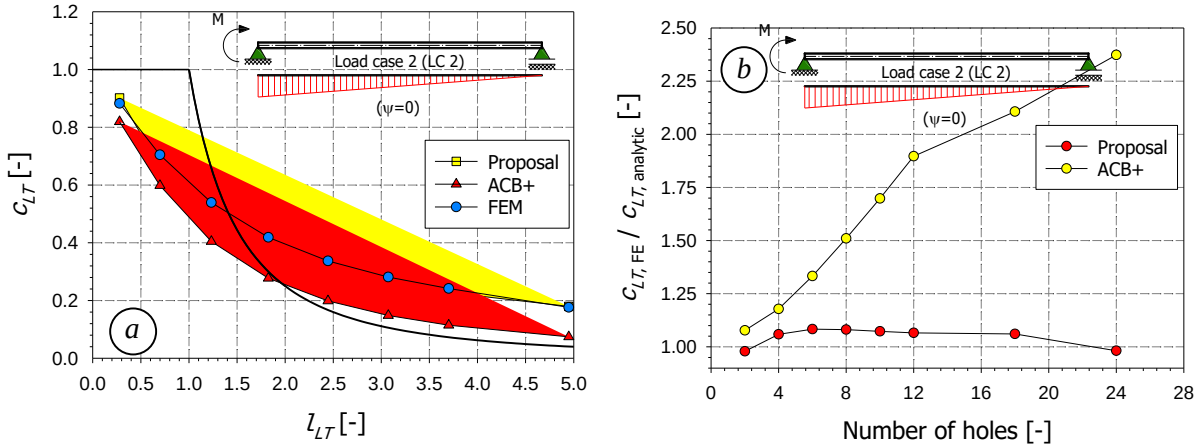

Fig. 15. Results for base profile IPE 600, triangular bending moment, s = 1.75 a_0, S235, curve *c*.

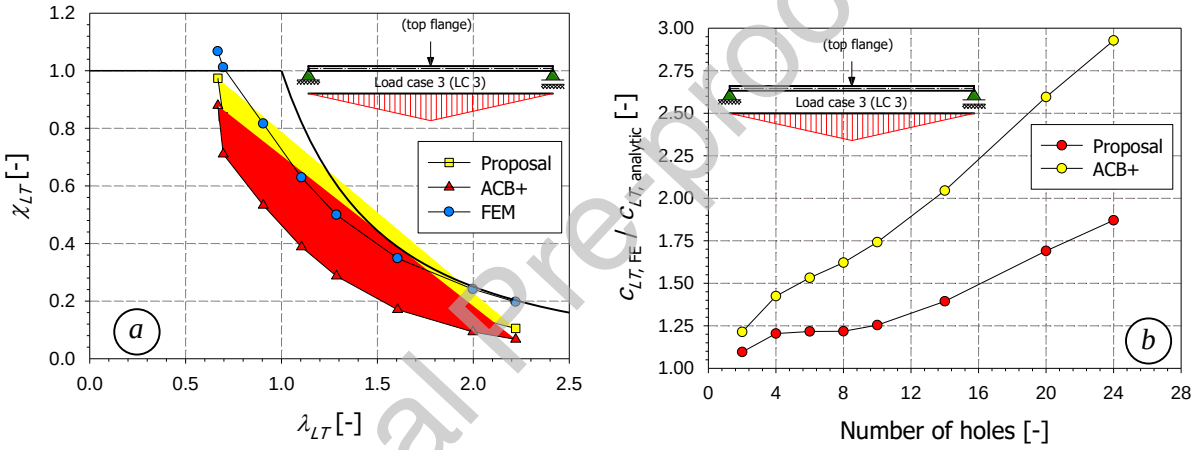

Fig. 16. Results for base profile IPE 600, concentrated load at mid-span, s = 1.75 a_0, S235, curve *c*.

Fig. 16 however shows less accurate results for the proposed approach in the case of a point load case, mostly owing to non-constant bending moment distributions. Resistance predictions tends to be more conservative, however still safe-sided and much more accurate than those of the ACB+ model. Especially, the change in s = 1.12 a_0 in Fig. 13 to s = 1.75 a_0 considered in Figs. 15 and 16 could be shown not to be responsible for the less accurate predictions, as Table 5 further shows. A detailed analysis of all results collected revealed that resorting to (i) other parent sections or to (ii) other load cases with non-constant bending moment distributions provide slightly better results than those of Fig. 16 – see example of Fig. 17 –, yet less good as for the

reference constant bending moment LC1 load case (see also Table 5). Yield extent along the longitudinal axis of the beam can be evidenced to lie at the basis of $\chi_{LT} \geq 1.0$ values in Fig. 17a, for λ_{LT} values up to $\lambda_{LT} \approx 0.8$. For higher λ_{LT} values, the proposed approach is seen to lead to quite safe resistance estimates, which are nonetheless much less conservative than ACB+ ones, which can reach up to 300% over-safety – meaning that the resistance according to ACB+ can be tripled to reach the actual one.

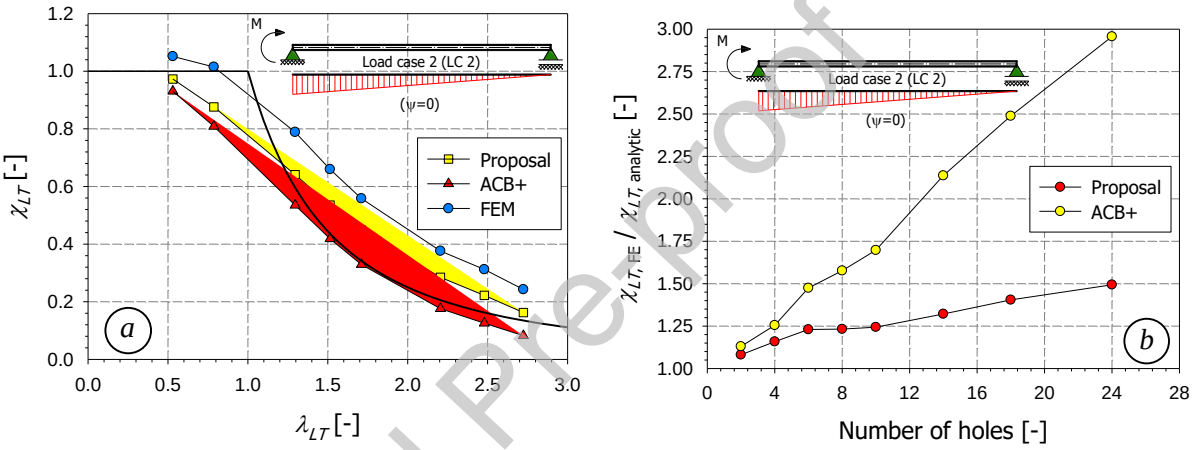

Fig. 17. Results for base profile IPE 300, triangular bending moment, s = 1.75 a_0, S235, curve c.

As a further illustration of the observed tendencies, Table 5 proposes statistical results of the comparison between numerical, "ACB+" and "proposal" results in terms of $\chi_{LT,FE}$ / $\chi_{LT,proposal}$ and $\chi_{LT,FE}$ / $\chi_{LT,ACB+}$ ratios, for the particular case of an IPE 600 base profile of steel grade S460. For each of these ratios, a value higher than 1.0 indicates a safe analytical estimate of the L.T.B. resistance while ratios ≤ 1.0 denote unsafe predictions. As can be seen, the resistance estimates are significantly improved by the new proposal, and the mean and standard deviation values also indicate a high level of consistency. This is further illustrated for other parent sections in the histograms of Fig. 18a and Fig. 18b, where (i) the F.E.-to-proposal ratio is more frequently closer to unity than the equivalent F.E.-to-ACB+ ratio (especially in Fig. 18a) and (ii) more consistent

predictions are provided by the proposed approach, as revealed by tighter distributions – a "perfect histogram" shall show a very narrow distribution slightly higher than 1.0. The comparison in these histograms clearly demonstrates the improved accuracy features of the proposed new rules, as well as a reduced scatter in the results. A detailed analysis of all available results in the parametric F.E. study confirms the observed trends, whatever the set of parameters. The proposed design rules are then seen to be much more accurate and consistent than the actual ACB+ ones, potentially leading to significant material savings for situations where lateral torsional buckling governs the design.

Table 5. Comparison between F.E., ACB+ and proposal results (base profile IPE 600, S460).

	Tot. FE results	$\chi_{LT,FE} / \chi_{LT,proposal}$				$\chi_{LT,FE} / \chi_{LT,ACB+}$			
		Min.	Max.	Mean	St. dev.	Min.	Max.	Mean	St. dev.
Load case 1	40	1.05	1.22	1.13	0.05	1.05	1.91	1.32	0.22
Load case 2	40	1.06	1.71	1.28	0.20	1.05	2.17	1.69	0.31
Load case 3	40	0.92	1.77	1.30	0.24	1.00	1.74	1.43	0.22
Load case 4	40	1.05	1.68	1.29	0.21	0.90	1.98	1.30	0.38
Load case 5	40	0.99	1.81	1.38	0.25	0.88	1.78	1.33	0.34
$s = 1.12\ a_0$	45	1.05	1.81	1.30	0.22	0.88	1.91	1.37	0.39
$s = 1.25\ a_0$	45	1.03	1.76	1.27	0.20	0.89	1.90	1.39	0.30
$s = 1.5\ a_0$	45	0.92	1.74	1.23	0.18	0.91	1.91	1.35	0.32
$s = 1.75\ a_0$	45	1.06	1.81	1.30	0.19	0.98	2.17	1.55	0.33

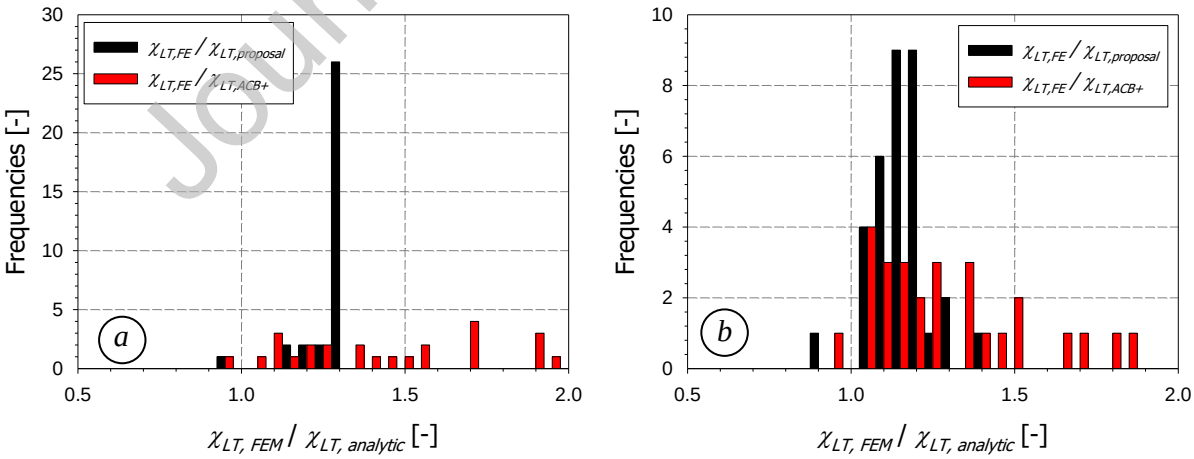

Fig. 18. Frequency distribution of $\chi_{LT,FE} / \chi_{LT,analytic}$ ratio – a) HEM1000, S235, constant bending moment distribution all relative sizes of openings s – b) IPE 300, S235, constant bending moment distribution, all relative sizes of openings s.

5. Conclusions

In this paper and a companion one [1], the lateral torsional buckling resistance of so-called "cellular" steel beams has been investigated, through both experimental, numerical and analytical (design) aspects. Since such girders usually meet their economical relevance for long spans, their resistance to L.T.B. is of prime importance and often leads the design. After showing an excellent agreement with the experimental results [1], the developed F.E. models have been further used in extensive parametric studies. In total, some 4 000 F.E. "reference" results have been gathered, accounting for the various influences of cross-sectional shape, bending moment distribution, relative size of the openings, and yield stress; they have further served as a database of reference results for assessing the merits of different design approaches.

The present paper also detailed a proposal for specific, improved design rules, which, in comparison with all the available F.E. results, was shown (i) to substantially improve the global accuracy of the design procedure – thus allowing for significant material savings – and (ii) to provide safe yet reasonably accurate estimates of the lateral torsional buckling resistance of such girders. Finally, comparisons with resistance predictions obtained from software ACB+ [31], which stands as the most highly used tool in design practice, demonstrated a significantly improved performance of the proposed design approach in terms of accuracy, consistency and reliability.

References

[1] Boissonnade, N., Nseir, J., Somja, H. (2023). "Experimental and numerical investigations towards the lateral torsional buckling of cellular steel beams". *Submitted to Thin-Walled Structures.*

[2] Radic, I., Markulak, D., Veravac, D. (2008). "Numerical simulation of lateral stability of castellated beams". *Proceedings of the 5th European Conference on Steel Structures, Eurosteel 2008, Graz, pp. 1593-1598, September 3-5*.

[3] El-Sawy, K, Sweedan, A., Martini, M. (2009). "Major-axis elastic buckling of axially loaded castellated steel columns". *Thin-Walled, Structures, 47, pp. 1295–1304.*

[4] Sweedan, A. (2011). "Elastic lateral stability of I-shaped cellular steel beams". *Journal of Constructional Steel Research, 67, pp 151–163.*

[5] Zirakian, T., Showkati, H. (2006). "Distortional buckling of castellated beams". *Journal of Constructional Steel Research, 62, pp. 863–871.*

[6] Ellobody, E. (2011). "Interaction of buckling modes in castellated steel beams". *Journal of Constructional Steel Research, Vo. 67 (814-825).* doi:10.1016/j.jcsr.2010.12.012.

[7] Verwij, J. (2010). "Cellular beam-columns in portal frame structures". *Master thesis, T.U. Delft.*

[8] Jian-zu Gu, Shanshan Cheng, "Shear effect on buckling of cellular columns subjected to axially compressed load", *Thin-Walled Structures 98 (2016) 416–420,* *http://dx.doi.org/10.1016/j.tws.2015.10.019*.

[9] Pattamad Panedpojaman, Worathep Sae-Long, Thaksin Thepchatri (2021), "Design of cellular beam-columns about the major axis", Engineering Structures 236, 112060, https://doi.org/10.1016/j.engstruct.2021.112060.

[10] Sonck, D., Vanlaere, R., Van Impe, R. (2010). "Elastic buckling of cellular members loaded by an axial force". *Proceedings of the International Association for Shell and Spatial Structures (IASS) Symposium 2010, Shanghai*.

[11] Sonck, D., Van Impe, R. (2011). "Elastic Buckling of Cellular Members Loaded by an Eccentric Axial Force". *Proceedings of the 6th European Conference on Steel Structures, Eurosteel 2011, Budapest, August 31 - September 2*.

[12] Melissa Kerkhove, "Global buckling of eccentrically loaded cellular members", *Master of Science in Civil Engineering, U Ghent, 2015.*

[13] Pattamad Panedpojaman, Thaksin Thepchatri, Suchart Limkatanyu (2014), "Novel design equations for shear strength of local web-post buckling in cellular beams", Thin-Walled Structures, Vol. 76 (92-104), http://dx.doi.org/10.1016/j.tws.2013.11.007

[14] Rabee Shamass, Federico Guarracino (2020), "Numerical and analytical analyses of high-strength steel cellular beams: A discerning approach", Journal of Constructional Steel Research 166 105911, https://doi.org/10.1016/j.jcsr.2019.105911.

[15] Caroline Correa de Faria, Hermes Carvalho, Ricardo Hallal Fakury, Lucas Figueiredo Grilo (2021), "Lateral-torsional buckling resistance of cellular steel beams at room temperature and fire situation", Engineering Structures 237, 112046, https://doi.org/10.1016/j.engstruct.2021.112046.

[16] Sonck, D. (2014), "Global buckling of castellated and cellular steel beams and columns". PhD Thesis, Ghent University.

[17] Delphine Sonck, Jan Belis (2015), "Lateral–torsional buckling resistance of cellular beams", *Journal of Constructional Steel Research 105 (2015) 119–128, http://dx.doi.org/10.1016/j.jcsr.2014.11.003*.

[18] Felipe Piana Vendramell Ferreira, Alexandre Rossi, Carlos Humberto Martins (2019), "Lateral-torsional buckling of cellular beams according to the possible updating of EC3", Journal of Constructional Steel Research 153 222–242, https://doi.org/10.1016/j.jcsr.2018.10.011.

[19] Pattamad Panedpojaman, Worathep Sae-Long, Tanan Chub-uppakarn. "Cellular beam design for resistance to inelastic lateral–torsional buckling", *Thin-Walled Structures 99(2016)182–194,* http://dx.doi.org/10.1016/j.tws.2015.08.026.

[20] Sharifi, Y.; Tohidi, S., "Lateral-torsional buckling capacity assessment of web opening steel girders by artificial neural networks—Elastic investigation". Front. Struct. Civ. Eng. 2014, 8, 167–177.

[21] Miguel Abambres, Komal Rajana, Konstantinos Daniel Tsavdaridis, Tiago Pinto Ribeiro (2019), "Neural Network-Based Formula for the Buckling Load Prediction of I-Section Cellular Steel Beams", Computers 2019, 8(1), 2; https://doi.org/10.3390/computers8010002.

[22] Felipe Piana Vendramell Ferreira, Rabee Shamass b, Vireen Limbachiya, Konstantinos Daniel Tsavdaridis, Carlos Humberto Martins (2022), "Lateral–torsional buckling resistance prediction model for steel cellular beams generated by Artificial Neural Networks (ANN)", Thin-Walled Structures 170, 108592, https://doi.org/10.1016/j.tws.2021.108592.

[23] Mohamed El Amine Ben Seghier, Hermes Carvalho, Caroline Correa de Faria, Jose´ A.F.O. Correia, Ricardo Hallal Fakury (2023), "Numerical analysis and prediction of lateral- torsional buckling resistance of cellular steel beams using FEM and least square support vector machine optimized by metaheuristic algorithms", Alexandria Engineering Journal, Volume 67, Pages 489-502, https://doi.org/10.1016/j.aej.2022.12.062.

[24] European Committee for Standardization (CEN) (2018). "PrEN 1993-1-1: Eurocode 3 – Design of Steel Structures – Part 1-1: General Rules and Rules for Buildings", Brussels.

[25] Gérard, L., Li, L., Kettler, M., and Boissonnade, N. (2021). "Steel I-Sections Resistance under Compression or Bending by the Overall Interaction Concept," Journal of Constructional Steel Research, 182, p. 106644.

[26] Greiner R., Kettler M., Lechner A., Freytag B., Linder J., Jaspart J.-P., Boissonnade N., Bortolotti E., Weynand K., Ziller C., Oerder R. (2007) "SEMI-COMP: plastic member capacity of semi-compact steel sections – a more economic design", Research Fund for Coal and Steel, European Commission, (ISBN 978-92-79-11113-6, 139 pages).

[27] Li, L., and Boissonnade, N. (2022). "Local/Global Coupled Instabilities of Slender I-Sections under Compression," Thin-Walled Structures, 172, p. 108842.

[28] Li, L., Paquet, J., Couto, C., Vila Real, P., and Boissonnade, N. (2023), "Fire local stability of steel I-sections under simple load cases", Engineering Structures 283, 115874, https://doi.org/10.1016/j.engstruct.2023.115874.

[29] Boissonnade, N., et H. Somja (2012). "Influence of Imperfections in FEM Modeling of Lateral Torsional Buckling", Proceedings of the Annual Stability Conference, SSRC. Grapevine, Texas.

[30] Gérard, L., Li, L., Kettler, M., and Boissonnade, N., 2019, "Recommendations on the Geometrical Imperfections Definition for the Resistance of I-Sections," Journal of Constructional Steel Research, 162, p. 105716. https://doi.org/10.1016/j.jcsr.2019.105716

[31] ACB+ (2022). ArcelorMittal Cellular Beams software ACB+ v4.02, Long Carbon Europe Research Centre.

Declaration of interests

☐ The authors declare that they have no known competing financial interests or personal relationships that could have appeared to influence the work reported in this paper.

☒ The authors declare the following financial interests/personal relationships which may be considered as potential competing interests:

Nicolas Boissonnade reports equipment, drugs, or supplies was provided by ArcelorMittal.

Author statement

We confirm that the manuscript has been read and approved by all named authors and that there are no other persons who satisfied the criteria for authorship but are not listed. We further confirm that the order of authors listed in the manuscript has been approved by all of us.